High-pressure Synthesis of Strontium Hexasilicide

Aron Wosylus, Yurii Prots, Ulrich Burkhardt, Walter Schnelle, Ulrich Schwarz, and
Yuri Grin

Max-Planck-Institut für Chemische Physik fester Stoffe, Nöthnitzer Straße 40, D-01187 Dresden,
Germany

Reprint requests to Dr. Ulrich Schwarz. E-mail: schwarz@cpfs.mpg.de

The binary phase $SrSi_6$ was prepared at a pressure of 10(1) GPa and a temperature of 1520(150) K. Single crystal refinements and powder diffraction data reveal that the compound crystallizes in the orthorhombic crystal system (*Cmcm*, $a = 4.4692(4)$, $b = 10.256(1)$, $c = 11.698(1)$ Å) and is isopointal to $EuGa_2Ge_4$ and $EuSi_6$. Exothermic decomposition of the compound into $SrSi_2$ and Si at 797 K and ambient pressure indicates that the compound is a metastable high-pressure phase. Analysis of the chemical bonding using the electron localization function and calculated charge densities reveals covalent bonding within the polyanion of four-bonded silicon atoms. Strontium cations are enclosed in the 3D net resulting in an electron balance $Sr^{2+}[Si^0]_6^{2-}$. In the electronic density of states the excess electrons of the framework are assigned to a filling of antibonding bands. $SrSi_6$ is a metallic conductor with an electrical resistivity of $\rho \approx 250\ \mu\Omega \cdot$cm at 300 K. Magnetization measurements indicate diamagnetic behaviour ($\chi_0 = -50 \cdot 10^{-6}$ emu·mol^{-1}).

Key words: Strontium, Silicon, High Pressure, Zintl Phase

Introduction

Anionic frameworks which are constituted of four-bonded post-transition main group elements are often semiconducting valence compounds in accordance with the $8 - N$ rule and the Zintl-Klemm concept. In polyanions comprising germanium or tin, an excess of electrons is often compensated by the formation of electron pairs around defects [1, 2] or by substitution of group 14 elements with group 13 atoms [3, 4]. Recently, $EuSi_6$ exhibiting an excess of two electrons per formula unit and a metal-type temperature dependence of the electrical conductivity was synthesized at high pressures and elevated temperatures [5]. Investigating the homogeneity range of the ternary substituted variety $EuGa_xSi_{6-x}$ ($x = 0 - 0.6$) reveals that the phase *requires* a significant excess of electrons since the composition $Eu[(4b)Ga^-]_2[(4b)Si^0]_4$ which would be in accordance with the $8 - N$ rule could not be realized experimentally. Since new phases comprising anionic frameworks of four-bonded atoms, like $EuSi_6$ [5] and $EuSi_{6-x}Ga_x$ [6, 7] or $BaSi_{6-x}$ [8, 9] can be prepared by application of high pressure, we have studied phase formation in the silicon-rich part of the phase diagram of the binary system Sr–Si at elevated pressures. Here we report on high-pressure synthesis, crystal structure, chemical bonding, magnetic properties, and electrical transport of the new binary compound $SrSi_6$.

Experimental Section

Synthesis

Preparation of the precursors and sample handling including the prearrangement of the octahedral high-pressure assemblies is performed in argon-filled glove boxes (MBraun, $H_2O < 1$ ppm; $O_2 < 1$ ppm). After preparing $SrSi_2$ by arc melting, the disilicide is mixed with silicon to realize ratios Sr : Si of 1 : 4, 1 : 6 or 1 : 8, respectively. In order to avoid contamination with oxygen, the high-pressure assembly is transferred to the press directly before synthesis. After the experiment, the set-up is immediately removed from the Walker module and transported into a glove box where the sample is recovered from the crucible.

High-pressure and high-temperature preparation is performed in an octahedral multianvil press. Force redistribution is realized by a Walker module and MgO octahedra with an edge length of 14 mm [10]. Elevated temperatures are realized by resistive heating of graphite tubes. Pressure and temperature calibration is performed prior to the experiments by *in situ* monitoring of the resistance changes of bismuth [11] and by performing calibration heating runs with a thermocouple, respectively. As crucible material enclosing the sample mixtures served hexagonal boron nitride. A reaction of the containers with the samples is not evidenced by X-ray

powder diffraction data or energy dispersive X-ray analysis. In accordance with this finding, the reaction products can be separated from the crucibles without difficulties. For the high-pressure syntheses, annealing times of one hour are typical. Single crystals grow at a pressure of 10(1) GPa and a temperature of 1520(150) K. Quenching to ambient temperature is realized by disconnecting the heating current before decompression.

Characterization

In order to investigate homogeneity and phase distribution of the samples by light- and electron-optical microscopy, the potentially water sensitive samples are prepared for the met-allographic study in an inert gas atmosphere of a glove box using dried hexane as a lubricant. The composition of the target phase is determined by wave-length dispersive X-ray spectroscopy (WDXS) on a microprobe (Cameca SX100). Pure silicon and the gallide $SrGa_4$ are used as references. The intensity of both lines SiK_α (E = 1736 keV) and SrL_α (E = 1807 keV) is used for calculations of the phase composition. Counting rates of 10000 cps (counts per seconds) on the spectrometer with a TAP monochromator crystal are adjusted by using an excitation voltage of 15 keV for the electron beam with 4 nA and 30 nA, respectively. An average of 10 points yields recoveries in the range of $100 - 99$ wt. %. The spectra up to 25 keV are determined by energy dispersive spectroscopy (EDXS) on an attached EDAX system and exhibit only the characteristic X-ray lines of Si and Sr. The composition of additional phases like Si or $SrSi_2$ is also verified by EDXS measurements.

Differential Scanning Calorimetry (DSC) measurements at ambient pressure are performed with the Netzsch DSC 404c equipment using Al_2O_3 crucibles at temperatures between 300 and 1520 K.

X-ray powder diffraction data are collected in transmission alignment with a Huber Image Plate Guinier Camera G670 employing CuK_{α_1} ($\lambda = 1.54056$ Å) radiation. In order to avoid oxidation during powder preparation, samples are ground in an inert atmosphere. After adding LaB_6 as an internal standard ($a = 4.1569$ Å) the mixture is fixed between two mylar foils. For lattice parameter refinements, sets of about 50 reflections are used. Profile fitting and lattice parameter calculations are performed with the program package WinCSD [12]. Structure refinements with single crystal diffraction intensity data are performed with the computer programs SHELXL-97 [13] and WinCSD. The parameters of data collection and refinement are shown in Table 1. Careful inspection of diffraction images does not evidence super-structure reflections. Final least squares calculations are performed using an anisotropic description of the displacement and weighting of the reflections by $1/\sigma^2$.

Magnetization at various external fields between 20 Oe and 70 kOe (temperature range 1.8 K – 400 K) is measured in

Table 1. Data collection and crystallographic information for $SrSi_6$[a].

Composition	$SrSi_6$
Temperature [K]	293
Crystal system/Space group	orthorhombic, *Cmcm* (no. 63)
Unit cell parameters[b]	
a [Å]	4.4692(4)
b [Å]	10.256(1)
c [Å]	11.698(1)
V [Å^3]	535.1(1)
Formula units/unit cell Z	4
Calculated density [g·cm^{-3}]	3.17
Size of the crystal [μm^3]	$8 \times 20 \times 25$
Diffractometer	Rigaku AFC 7
Detector	Mercury CCD
Wavelength λ(MoK_α) [Å]	0.71073
Scan, step/deg	$\phi, \omega = 0.6$
$2\theta_{max}$ [deg]	59.24
Range in h, k, l	$-6 \leq h \leq 5$
	$-13 \leq k \leq 13$
	$-16 \leq l \leq 16$
Transmission factors T_{max}/T_{min}	1.57
Number of measured reflections	2145
Number of unique reflections	433
R(int)	0.043
Number of observed reflections	394
Observation criterion	$F(hkl) > 4\sigma(F)$
Number of parameters	24
$R(F)$	0.032
Residual density / e Å^{-3}	$-0.54/0.76$
Extinction coefficient	0.0007(1)

[a] Further details on the crystal structure investigations can be obtained from the Fachinformationszentrum Karlsruhe, D-76344 Eggenstein-Leopoldshafen, Germany, fax:(+49)7247-808-666; e-mail: crysdata@fiz.karlsruhe.de, on quoting the depository number CSD 416971; [b] from powder diffraction data.

a SQUID magnetometer (MPMS XL-7, Quantum Design) on a polycrystalline sample (mass $m \sim 8$ mg). On the same sample an electrical resistivity measurement is performed with a *dc* four-point method (4 K – 320 K). Due to the small size of the piece the inaccuracy of the absolute resistivity values is estimated to be $\pm 30\%$.

Calculation procedure

Electronic structure calculation and bonding analysis for $SrSi_6$ are carried out using the TB-LMTO-ASA program package [14]. The Barth-Hedin exchange potential [15] is employed for the LDA calculations. The radial scalar-relativistic Dirac equation is solved to get the partial waves. The calculation within the atomic sphere approximation (ASA) includes corrections for the neglect of interstitial regions and partial waves of higher order [16], an addition of empty spheres is in case of $SrSi_6$ not necessary. The following radii of the atomic spheres are applied for the calculations on $SrSi_6$: $r(Sr) = 2.345$ Å, $r(Si1) = 1.441$ Å, $r(Si2) = 1.410$ Å, $r(Si3) = 1.461$ Å. A basis set containing $Sr(5s, 4d)$ and
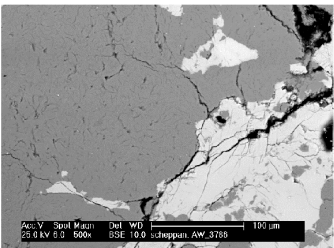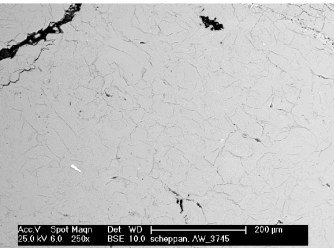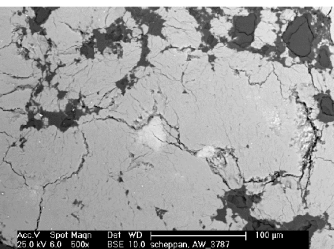
Composition and unit cell parameters (Å)	Microstructure
Nominal composition of the sample: $SrSi_4$ WDXS for $SrSi_6$ phase: $Sr_{1.000(2)}Si_{5.9(1)}$ $a = 4.470(1)$ $b = 10.264(3)$ $c = 11.699(3)$	
Nominal composition of the sample: $SrSi_6$ WDXS for $SrSi_6$ phase: $Sr_{1.000(3)}Si_{5.9(1)}$ $a = 4.4692(4)$ $b = 10.256(1)$ $c = 11.698(1)$	
Nominal composition of the sample: $SrSi_8$ WDXS for $SrSi_6$ phase: $Sr_{1.000(2)}Si_{5.8(1)}$ $a = 4.4688(9)$ $b = 10.259(2)$ $c = 11.701(2)$	

Fig. 1. Microstructures of samples in the silicon-rich part of the Sr–Si phase diagram after high-pressure treatment (see text). The pictures present back scattering electron images recorded with a scanning electron microscope; grey areas indicate $SrSi_6$, light grey $SrSi_2$, and dark grey Si.

$Si(3s, 3p)$ orbitals is employed for a self-consistent calculation with $Sr(5p, 4f)$ and $Si(3d)$ functions being downfolded.

The electron localization function (ELF, η) and electron localizability indicator (ELI), Y are evaluated according to [17] and [18] with an ELF module implemented within the TB-LMTO-ASA program package [14]. The topology of ELF is analyzed using the program Basin [19] with consecutive integration of the electron density in basins which are bound by zero-flux surfaces in the ELF gradient field. The integration is performed numerically on the grid with a step width of 0.03 Å. This procedure, similar to the one proposed by Bader for the electron density [20], allows to assign an electron count for each basin, revealing the basic information about the chemical bonding.

Results and Discussion

As a lower limit for the formation of $SrSi_6$ a pressure of 5.0(5) GPa is observed. With respect to WDX measurements, the composition of the investigated samples is 1 : 5.9(1) and, thus, in accordance with a 1 : 6 compo-

Table 2. Atomic coordinates and displacement parameters of SrSi$_6$ at 293 K. The U_{eq} values (in Å^2) are defined as one third of the trace of the U_{ij} tensor, the total displacement is defined as $\exp -2\pi^2[U_{11}h^2a*^2+\ldots+2U_{23}klb*c*]$. For all positions $U_{12}=U_{13}=0$.

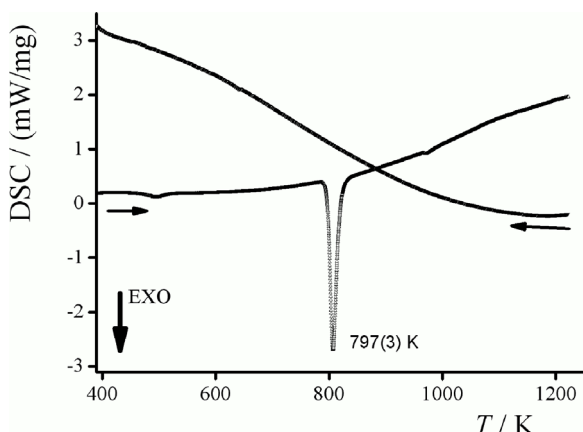| Atom	Site	x	y	z	U_{eq}	U_{11}	U_{22}	U_{33}	U_{23}
Sr	4c	0	0.27214(8)	1/4	0.0142(2)	0.0172(4)	0.0130(4)	0.0125(4)	0
Si1	8g	0	0.2472(2)	0.5380(1)	0.0104(4)	0.0069(6)	0.0138(8)	0.0104(6)	0.0001(6)
Si2	8g	0	0.5577(1)	0.3527(1)	0.0106(4)	0.0122(7)	0.0095(7)	0.0102(6)	−0.009(6)
Si3	8g	0	0.0235(1)	0.6010(1)	0.0112(4)	0.0077(7)	0.0111(8)	0.0147(6)	0.0004(6)

Fig. 2. Differential scanning calorimetry measurement of SrSi$_6$ at ambient pressure. With increasing temperature, the decomposition of the metastable high-pressure phase SrSi$_6$ into the products SrSi$_2$ and Si which are thermodynamically stable at ambient pressure is detected by an exothermic peak at 797(3) K (onset temperature).
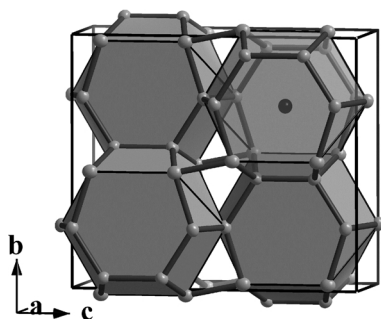

Fig. 3. Crystal structure of SrSi$_6$. The framework is formed by three crystallographically independent silicon atoms which are connected by covalent bonds. The voids of the 3D silicon network are occupied by strontium. The coordination polyhedron of the alkaline earth metal with CN 18 is indicated by shading.

sition found in the crystal structure analysis. In order to investigate the homogeneity range, three samples are synthesized which are located in the silicon-rich part of the binary Sr–Si phase diagram: one with an exact composition Sr : Si = 1 : 6, one with an excess of sil-

Table 3. Interatomic distances for SrSi$_6$.

Atoms			d, Å	Atoms			d, Å
Si1	–	Si2	2.374(2)	Si1	–	Si1 (2×)	2.401(1)
Si1	–	Si3	2.411(2)	Si2	–	Si1	2.374(2)
Si2	–	Si2	2.403(2)	Si2	–	Si3 (2×)	2.441(1)
Si3	–	Si1	2.411(2)	Si3	–	Si3	2.412(4)
Si3	–	Si2 (2×)	2.441(1)	Sr	–	Si2 (2×)	3.166(2)
Sr	–	Si1 (4×)	3.341(1)	Sr	–	Si2 (4×)	3.355(1)
Sr	–	Si1 (2×)	3.379(1)	Sr	–	Si3 (2×)	3.497(2)
Sr	–	Si3 (4×)	3.522(1)	Sr	–	Sr (2×)	4.4602(8)

icon (1 : 8) and another one with a significant deficit (1 : 4) under the same pressure and temperature conditions of 10(1) GPa and 1520(150) K. The result of the metallographic investigation reveals that the sample Sr : 4 Si contains SrSi$_2$ together with the hexasilicide (Fig. 1). The SrSi$_6$ sample is basically single-phase. In the SrSi$_8$ sample, elemental silicon was found beside the SrSi$_6$ compound. The refined lattice parameters of the SrSi$_6$ phase for different nominal compositions are equal within 3 e.s.d.'s (see Fig. 1). This is taken as evidence for a constant composition of the hexasilicide.

The thermal stability of SrSi$_6$ is studied at ambient pressure by means of DTA measurements. The investigation reveals a pronounced exothermic signal at 797(2) K (onset) which does not correspond to a thermal effect upon cooling (Fig. 2). This observation is compatible with a monotropic (irreversible) phase transition. X-ray powder diffraction data of samples which are investigated after the heating cycle exhibit only diffraction lines of Si and SrSi$_2$. Thus, the experiments are consistent with a decomposition of SrSi$_6$ at 797(2) K and atmospheric pressure, indicating that the compound is a metastable high-pressure phase under ambient conditions.

The crystal structure of SrSi$_6$ is refined by means of X-ray single crystal diffraction data. Atomic coordinates and displacement parameters are summarized in Table 2, interatomic distances in Table 3. The atomic arrangement is isopointal to EuGa$_2$Ge$_4$ [6, 7] and EuSi$_6$ [5]. The 3D network consists of four-bonded
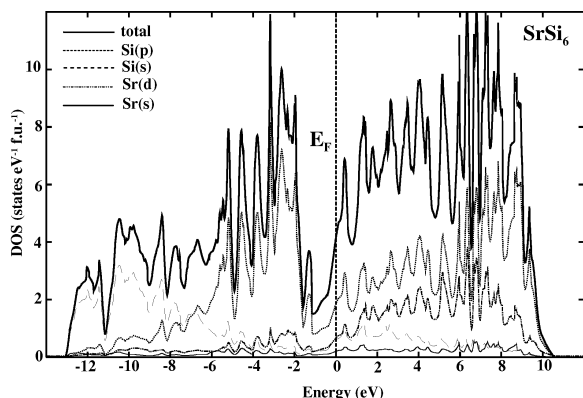
Fig. 4. Electronic density of states for SrSi$_6$ with partial contributions of the Sr(s), Sr(d), Si(s) and Si(p) states.

Si atoms enclosing large voids which are occupied by strontium atoms (Fig. 3).

The previously known binary compounds in the phase diagram strontium−silicon are α-SrSi$_2$ (α-ThSi$_2$-type) and β-SrSi$_2$ (with its own structure type), two modifications of SrSi (CrB structure type, also labelled as α-TlI, and of its own structure type, respectively), Sr$_5$Si$_3$ (Cr$_5$B$_3$-type) and Sr$_2$Si (PbCl$_2$-type) at normal pressure [21]. All binary compounds are Zintl Phases with closed-shell configuration of the constituents, *i. e.*, formally a complete valence electron transfer from strontium to silicon takes place. However, SrSi and SrSi$_2$ exhibit metallic conductivity. With respect to the electron count, the phases fulfil the $8 − N$ rule so that these compounds are *silicides* composed of Sr^{2+} and isolated Si$^{4−}$in Sr$_2$Si [22], isolated Si$^{4−}$ and (1b)Si$^{3−}$ (Si$_2^{6−}$ dumbbells) in Sr$_5$Si$_3$ [23, 24], (2b)Si$^{2−}$ chains in SrSi [25, 26] or a mixture of (1b)Si$^{3−}$, (2b)Si$^{2−}$ and (3b)Si$^−$ in a second modification of SrSi comprising condensed-chain fragments [27], and finally (3b)Si$^−$ in the networks of dimorphic SrSi$_{2−x}$ [28 − 32]. The 3D network in the new compound SrSi$_6$ is formed by four-bonded silicon atoms (4b)Si^0. Thus, with respect to the $8 − N$ rule there is an excess of two electrons per formula unit like in the homologous compound EuSi$_6$ [5]. In order to investigate this unusual bonding situation in more detail, the electron count is investigated by quantum chemical calculations.

The electronic density of states (DOS) for SrSi$_6$ reveals a *pseudo* gap just below the Fermi level (Fig. 4). The bonding region of DOS ($E < −1$ eV) is formed by the Sr(s) states together with Si(s) for $E < −6$ eV and Si(p) states for $−6 < E < −1$ eV. In a hypo-

thetical 3D framework of uncharged four-bonded silicon atoms with two-centre two-electron bonds, only bonding states below the *pseudo* gap would be filled. Nevertheless, in case of Sr[(4b)Si$_6$], a fraction of the anti-bonding band is also occupied. This part of the DOS is formed mainly by the Sr(d), and Si(p) states with minor admixtures of Sr(s) and Si(s) states. The occupation of the antibonding states leads to a distinct high density of states at the Fermi level suggesting metallic behaviour in the transport properties (see below).

In order to gain more detailed insight into the chemical bonding, the electron localization function and the electron localizability indicator are calculated according to the procedure described above. The topology of both bond-indicating functions is found very similar in case of SrSi$_6$, thus we present here only the ELF data in order to be compatible with the results on europium hexasilicide [5]. The electron localization function reveals three nearly fully spherical closed shells around the strontium position, indicating the transfer of the electrons of the fourth shell to the silicon framework (Fig. 5, top). In addition, no unique ELF attractor is found between the strontium and the framework silicon atoms, supporting the picture of mainly ionic interactions between the cations and the anionic framework.

Maxima of ELF are found only in the vicinity of the Si–Si contacts, as visualized by the isosurface of $\eta = 0.775$ (Fig. 5, bottom). According to the position of the attractors and taking into account only silicon atoms, each of the Si–Si bonds seems to be a two-centre interaction. The shift of the Si–Si attractors towards strontium positions correlates with the picture of charge transfer and illustrates the kind of participation of the cations in these interactions. A more careful analysis reveals that the basins of all Si–Si bonds – except Si3–Si3 – are in contact with the inner shell of strontium (Fig. 5). Integration of the electron density within the ELF basins gives counts slightly larger than two for all bonds except Si3-Si3 which comprises less than two electrons. It is noteworthy that there is no correlation between the size of interatomic distances in the silicon network and the corresponding electron counts (Fig. 6). A simple qualitative picture of the chemical bonding would predict solely two-centre two-electron interactions for four-bonded silicon atoms. Thus, the electron counts for Si-Si bonds larger than two indicates a different kind of bonding in comparison, *e. g.*, with elemental silicon.
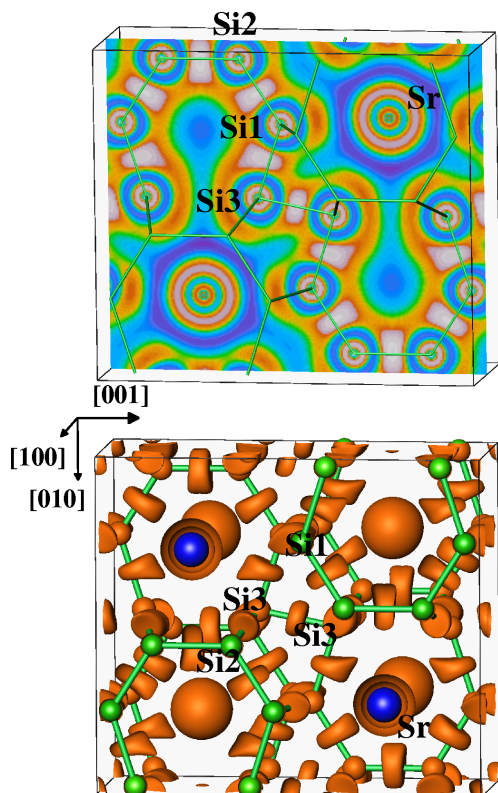
Fig. 5. Electron localization function in SrSi$_6$: Section at $x = 0.5$ (top) and isosurface with $\eta = 0.775$ (bottom).

In total, the chemical bonding in SrSi$_6$ within the Zintl-Klemm concept is considered to be represented by the charge balance SrSi$_6$ = [Sr^{2+}] [(4b)Si$_6^0$] ·2e$^-$. Application of the combined approach of ELF/ELI with electron density reveals a slightly different charge balance: SrSi$_6$ = [Sr$^{1.86+}$] [(4b)Si$_6$]$^{1.86-}$ evidencing that the compound does not belong to the class of original Zintl Phases, but represents a member of the group of electron-excess intermetallic compounds which are frequently labelled as metallic Zintl Phases [33, 34].

In accordance with this, the resistivity $\rho(T)$ of SrSi$_6$ (Fig. 8) increases linearly with temperature for $T >$ 50 K indicating a metallic conduction mechanism. At 300 K a value of 250 $\mu\Omega$·cm and at 4 K a residual resistivity of 50 $\mu\Omega$·cm is observed. These are relatively low resistivity values as compared with europium hexasilicide [5]. No superconductivity is found above 1.8 K.

The magnetic susceptibility $\chi(T) = M/H$ of SrSi$_6$ is almost independent of temperature. After taking into account minor para- and ferromagnetic impurities
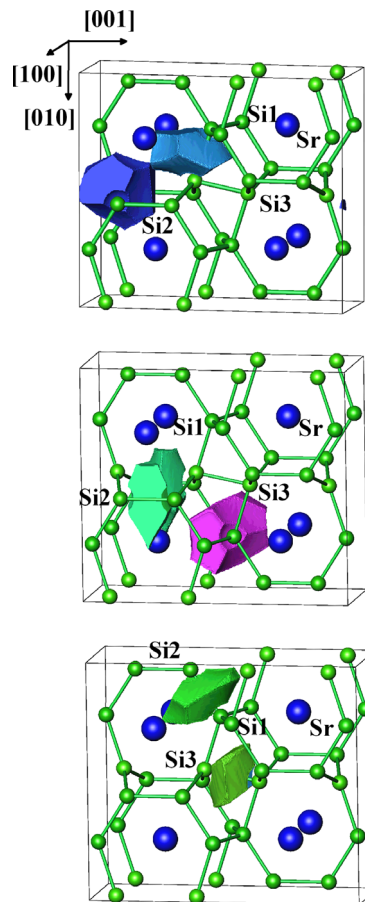

Fig. 6. Basins for bonding ELF attractors in the silicon framework of the crystal structure of SrSi$_6$: Si1–Si3 (top), Si2–Si3 (top), Si2–Si2 (middle), Si1–Si1 (middle), Si1–Si2 (bottom), Si3–Si3 (bottom).
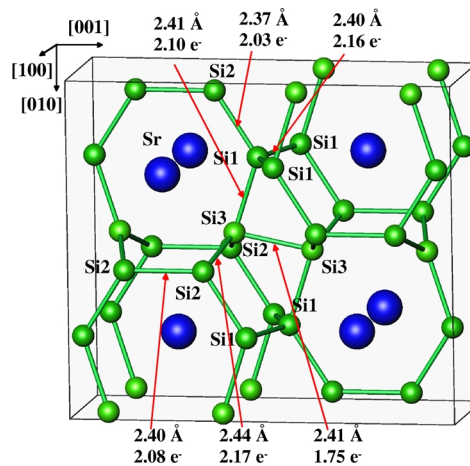

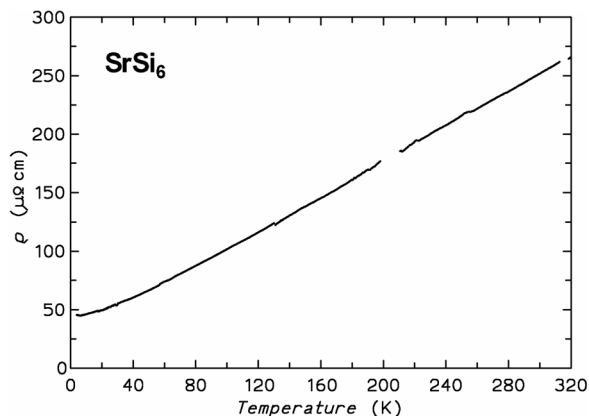Fig. 7. Bond lengths and electron counts for Si–Si bonds in the crystal structure of SrSi$_6$.

Fig. 8. Electrical resistivity of a polycrystalline sample of SrSi$_6$ *versus* temperature. The linear increase with temperature above approximately 100 K indicates metal-like conductivity.

(by a Curie term and by Honda-Owen extrapolation, respectively) a constant value of $\chi_0 = -50(10) \cdot 10^{-6}$ emu $\cdot$ mol^{-1} is obtained.

Conclusion

In the binary system Sr–Si, the new metastable phase SrSi$_6$ is prepared by high-pressure synthesis at elevated temperatures. A chemical bonding analysis by means of ELF calculations and integration of the electron density in ELF basins reveals an electron excess of the polyanionic silicon framework. This finding is in accordance with the experimentally determined diamagnetism and the metal-type conductivity.

[1] H. G. von Schnering, Nova Acta Leopoldina **59**, 168 (1985).

[2] J. Llanos, PhD Thesis, University of Stuttgart, 1984.

[3] B. Eisenmann, H. Schäfer, R. Zahler, J. Less-Common Met. **118**, 43 (1986).

[4] H. Anno, M. Hokazono, M. Kawamura, J. Nagao, K. Matsubara, in: Proc. Of the 21st Int. Conf. on Thermoelectrics, IEEE, p. 77, New York (2002).

[5] A. Wosylus, Yu. Prots, U. Burkhardt, W. Schnelle, U. Schwarz, Yu. Grin, Solid State Science **8**, 773 (2006).

[6] J. D. Bryan, G. D. Stucky, Chem. Mater. **13**, 253 (2001).

[7] W. Carrillo-Cabrera, S. Paschen, Yu. Grin, J. Alloys Compd. **333**, 4 (2002).

[8] R. Demchyna, S. Leoni, H. Rosner, U. Schwarz, Z. Kristallogr. **221**, 420 (2006).

[9] S. Yamanaka, S. Maekawa, Z. Naturforsch. **61b**, 1493 (2006).

[10] D. Walker, M. A. Carpenter, C. M. Hitch, Am. Mineral. **75**, 1020 (1990).

[11] D. A. Young, Phase diagrams of the elements, UC Press, 1991.

[12] L. G. Akselrud, P. Y. Zavalij, Yu. Grin, V. K. Pecharsky, B. Baumgartner, E. Wölfel, Material Science Forum **133 – 136**, 335 (1993).

[13] G. M. Sheldrick, SHELXL-97 – A program for crystal structure refinement, University of Göttingen, Release 9772, Germany (1997).

[14] O. Jepsen, A. Burkhardt, O. K. Andersen, The Program TB-LMTO-ASA. Version 4.7. Max-Planck-Institut für Festkörperforschung, Stuttgart (1999).

[15] U. Barth, L. Hedin, J. Phys. C **5**, 1629 (1972).

[16] O. K. Andersen, Phys. Rev. B **12**, 3060 (1975).

[17] A. Savin, H. J. Flad, H. Preuss, H. G. von Schnering, Angew. Chem. **104**, 185 (1992); Angew. Chem. Int. Ed. Engl. **31**, 185 (1992).

[18] M. Kohout, Int. J. Quant. Chem. **97**, 651 (2004).

[19] M. Kohout, Basin. Version 2.3. Max-Planck-Institut für Chemische Physik fester Stoffe, Dresden (2001).

[20] R. F. W. Bader, Atoms in molecules: a quantum theory, Oxford University Press, Oxford (1999).

[21] A. Palenzona, M. Pani, J. Alloys Comp. **373**, 214 (2004).

[22] A. Widera, B. Eisenmann, Z. Naturforsch. **31b**, 520 (1976).

[23] E. A. Leon-Escamilla, J. D. Corbett, J. Solid State Chem. **159**, 149 (2001).

[24] R. Nesper, F. Zürcher, Z. Kristallogr. NCS **214**, 19 (1999).

[25] G. Rocktaschel, A. Weiss, Z. Anorg. Allg. Chem. **316**, 231 (1962).

[26] B. Eisenmann, H. Schäfer, Z. Naturforsch. **29b**, 464 (1974).

[27] B. Eisenmann, H. Schäfer, K. Turban, Z. Naturforsch. **29b**, 460 (1974).

[28] K. H. Janzon, H. Schäfer, Z. Naturforsch. **22b**, 100 (1967).

[29] K. H. Janzon, H. Schäfer, A. Weiss, Z. Anorg. Allg. Chem. **372**, 87 (1970).

[30] J. Evers, G. Oehlinger, A. Weiss, J. Solid State Chem. **20**, 173 (1977).

[31] J. Evers, J. Solid State Chem. **24**, 199 (1978).

[32] M. Imai, T. Kikegawa, Chem. Mater. **15**, 2543 (2003).

[33] R. Nesper, Prog. Solid State Chem. **20**, 1 (1990).

[34] J.-T. Zhao, J. D. Corbett, Inorg. Chem. **34**, 378 (1995).